Conformational Analysis of L-Prolines in Water

Abil E. Aliev* and Denis Courtier-Murias

Department of Chemistry, University College London, 20 Gordon Street, London WC1H 0AJ, United Kingdom

Received: August 22, 2007

The results of the ring conformational analysis of L-proline, *N*-acetyl-L-proline, and *trans*-4-hydroxy-L-proline by NMR combined with calculations using density functional theory (DFT) and molecular dynamics (MD) are reported. Accurate values of $^1H-^1H$ *J*-couplings in water and other solvents have been determined. Using a two-site equilibrium model, the C^γ-endo conformer of L-proline in water has been identified as intermediate between ${}_\gamma T^\delta$ [twist(C^γ-endo, C^δ-exo)] and ${}_\gamma E$ [envelope(C^γ-endo)] and the C^γ-exo conformer as ${}_\beta T^\gamma$. Both conformers were equally populated at room temperature. The *N*-acetyl [*cis*-rotamer ${}_\gamma T^\beta$(80%)/${}^\gamma E$(20%) and *trans*-rotamer ${}_\gamma T^\beta$(61%)/${}^\gamma E$(39%)] and 4-hydroxy (${}^\gamma E$) derivatives showed significant changes in both the population and the geometries of the preferred ring conformers. The combination of NMR predicted populations with the DFT B3LYP/6-311+G(2d,p)/IEFPCM calculations proved successful, resulting in fairly accurate predictions of *J*-couplings. Simulations using MD were mostly in favor of the two-site equilibrium model between C^γ-endo and C^γ-exo conformers, similar to that used for the analysis of NMR *J*-couplings. Various force fields examined for MD simulations failed to reproduce the ring conformational geometries and populations of L-proline in water accurately, while significantly better agreement with NMR was found for *trans*-*N*-acetyl-L-proline using GROMOS and AMBER force fields.

Introduction

Conformational flexibility of L-proline, one of twenty natural amino acids with a unique cyclic structure, has attracted a considerable amount of research in the past.[1] Recently, there has been a renewed interest in neutral and zwitterionic L-proline and its hydroxylated derivative, *trans*-4-hydroxy-L-proline,[2] partly driven by the extensive developments of computational techniques, such as model calculations in aqueous solutions using density functional theory (DFT)[3] or molecular dynamics (MD) simulations of peptides and proteins.[4] Despite significant recent advances, any reliable MD simulation still depends critically on the force field parametrizations of amino acid residues, including Pro and Hyp,[5] which in turn rely on the availability and the accuracy of the experimental data reported for amino acids and their simple derivatives.

The renewed interest in simple L-prolines is also stimulated by the expansion of collagen research.[6] Formation of the triple helix conformation in collagen requires the presence of a repeated -Gly−X−Y− sequence, the most common sequence being -Gly-Pro-Hyp-. The ring puckering of the Pro residue[7] and the ratio of the *trans*- and *cis*-rotamers about the peptide bonds involving cyclic nitrogens of Pro residues[8] are important factors influencing the stability of collagen triple helices. Another important attribute of the L-proline residue is its hingelike function, which enhances the probability of β-turns in proteins.[1] This and other distinct properties are likely to be driven by the flexibility of the pyrrolidine ring in L-prolines, the understanding of which is far from being trivial despite the relative simplicity of the system.[2b] It will suffice to compare solid-state structures of L-proline,[9a] its monohydrate,[9b] DL-proline,[9c] and *trans*-4-hydroxy-L-proline,[9d] where the ring conformations are unusually dissimilar (Figure 1).

Even more obscure is the situation in the solution state, where fast interconversions of the flexible ring conformations of L-prolines are common (Figure 2) and, as identified previously,[1] there are 18 different envelope and twist conformations of the pyrrolidine ring. Such a situation is further instigated by the absence of powerful experimental techniques suitable for solution structure determinations.

NMR is well-known to be one of the highly favored methods suitable for studies of dynamic systems in solutions. However, being a spectroscopic technique, NMR relies on the interpretation of the measured parameters, which in turn may suffer from being model-dependent or simply inaccurate. Despite their small molecular size, L-prolines often show relatively complex NMR spectra. In particular, a combination of close proton chemical shifts and a large number of ^{2-4}J-couplings for each cyclic proton leads to a strongly coupled ^1H NMR spectrum, where unlike a first-order spectrum an observed splitting in a multiplet is not equal to a *J*-coupling and a full iterative analysis is required for the accurate determination of the NMR parameters.[10] Surprisingly, no such analysis of proton NMR spectra of L-proline or its *N*-acetyl derivative in aqueous solution has been reported previously. Reminiscent of high-resolution X-ray refinements, the highest possible accuracy of the NMR data is of principal importance for structure elucidation in the solution phase. We have therefore undertaken detailed NMR studies of L-prolines. Here, we present the results of our full NMR line shape analysis for L-proline and its *N*-acetyl and 4-hydroxy derivatives in water, followed by the derivation of their conformational geometries and populations, and comparison of MD force fields and DFT calculations in predicting the preferred ring conformations and NMR *J*-couplings.

Experimental Section

L-Proline, *N*-acetyl-L-proline (NAcPro), and *trans*-4-hydroxy-L-proline were purchased from Sigma-Aldrich and were used

* Tel: (+44) 020 7679 4616; Fax: (+44) 020 7679 7463; E-mail: a.e.aliev@ucl.ac.uk.

10.1021/jp076729c CCC: $37.00
Published on Web 11/21/2007

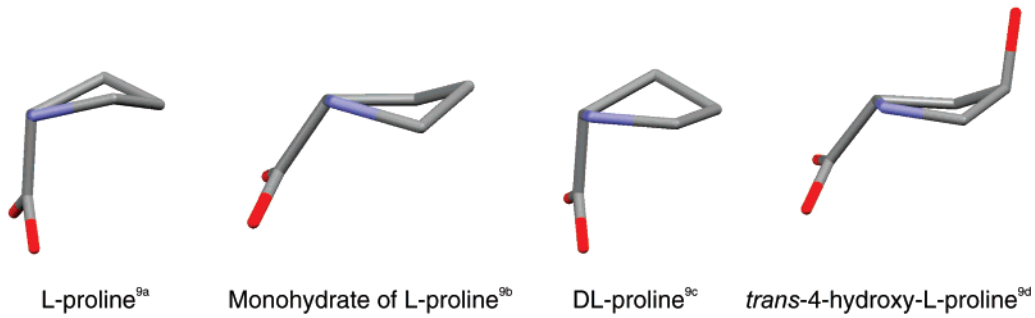

Figure 1. Four different conformations of the pyrrolydine ring found in single crystals.

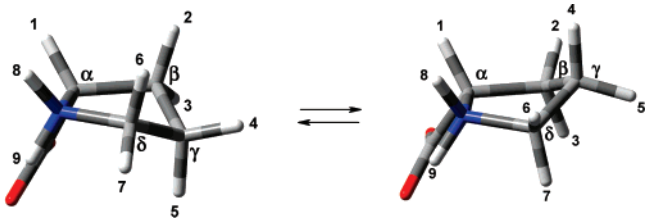

Figure 2. An example of a two-site equilibrium between down- (C^{γ}-endo, relative to CO_2, left) and up-puckered (C^{γ}-exo, right) conformers illustrated for zwitterionic L-proline together with the proton numbering and carbon labeling used.

without further purification. The pD of solutions in D_2O was measured using Corning pH meter 240 (pD = pH[meter reading] + 0.4).[11]

Solution ^{1}H spectra were recorded on Bruker NMR spectrometers AMX400 and AVANCE500 equipped with Bruker 5 mm BBO (broadband observation) probes. A proton NMR spectrum of L-proline in D_2O was also recorded on Bruker NMR spectrometer AVANCE700. Data acquisition and processing were performed using standard Bruker *XwinNMR* software (version 2.6). ^{1}H chemical shifts in D_2O were calibrated using sodium 3-(trimethylsilyl)propionate (TSP, 0 ppm) and dioxane (3.75 ppm). ^{1}H chemical shifts in other solvents were calibrated using residual solvent peaks (3.31 ppm in CD_3OD, 2.50 ppm in DMSO-d_6, and 7.26 ppm in $CDCl_3$).

Iterative full line shape analyses were carried out using gNMR.[12] Both the magnitude and the sign of the long-range couplings were allowed to vary in iterative line shape fittings. Least-squares fittings of the vicinal ^3J-couplings was carried out using a Fortran program based on an approach similar to that described previously,[1] but using a simulated annealing algorithm,[13] and eqs 8C and 8D of Haasnoot et al.[14] These equations contain terms accounting for the differences in electronegativities of α- and β-substituents, and hence are better suited for the analysis of the ^3J-couplings in prolines than the original Karplus equation.[15] The performance of the program was additionally verified using data from Table 6 of Haasnoot et al.[1] The RMS deviation defined as $1/N \sum_{i=1}^{N} (J^i_{exp} - J^i_{calc})^2$ was used as a figure-of-merit function, where J^i_{exp} and J^i_{calc} are experimental and calculated couplings, respectively, and N is the number of different J-couplings available.

Computational Methods

DFT Calculations. Geometry optimizations were carried out using B3LYP functional at the 6-31G(d), 6-311++G(2df,2pd), and cc-pvTZ levels as implemented in *Gaussian 03*.[16] Spin−spin couplings were computed using B3LYP at 6-311+G(2d,p) and 6-311++G(2df,2pd) levels. Solution-phase calculations in water used the IEFPCM model.[17]

MD Calculations. One molecule of zwitterionic L-proline or *trans*-*N*-acetyl-L-proline (either neutral or a CO_2^- terminated *trans*-NAcPro molecule with a Na^+ cation added for neutralization) surrounded by >800 water molecules in a cubic box were used in MD simulations with periodic boundary conditions. The structures used were energy-minimized, and the water molecules were allowed to relax (with positionally restrained solute) prior to MD production steps. The force fields employed were: GROMOS 53a6[18] (SPC water),[19] OPLS-AA[20] (TIP4P water),[21] AMBER[22,23] (TIP3P water),[21] and a general AMBER force field (GAFF,[24] TIP3P water). Apart from GAFF, *Gromacs* (version 3.3.1)[25] implementations of the force fields were used. Calculations using GAFF were carried out by AMBER (version 9).[26]

In simulations using *Gromacs*, neighbor lists were updated every fifth step. A cubic box of $3 \times 3 \times 3$ nm^3 was used. An integration step employed was 1 or 2 fs. Cutoff distances were different for different force fields.[18,20,22] Either the PME (particle mesh Ewald)[27] or the reaction field[28] corrections were used for the long-range electrostatic interactions. Langevin dynamics, with a reference temperature of 300 K and a weak frictional constant of 10 ps^{-1}, was employed in the majority of simulations.[29] In addition, Nose−Hoover and Berendsen temperature regulations[27−32] at 300 K were also used in some of the simulations. A Berendsen scheme was employed for pressure control at 1 bar using a coupling constant of 0.5 or 1 ps.[32] Prior to production runs, the system was minimized using L-BFGS, steepest-descent, and conjugate gradient algorithms. Minimization steps were followed by three stages of equilibration. The system was first equilibrated for 40 ps with the positionally restrained solute molecule to allow water molecules to equilibrate around it, followed by an *NVT* molecular dynamics for 10 ps without restraints and then by 100 ps of *NPT* dynamics with an isothermal compressibility of 4.5×10^{-5} bar^{-1} and a reference pressure of 1.0 bar. Production simulations were performed for 0.5−10 ns using mainly *NPT* ensemble. Further *NVT* calculations (5−10 ns) were also undertaken in some cases. The MD calculations using GAFF were performed using conditions similar to QM/MD described below. The average ^3J-couplings were calculated using eqs 8C and 8D of Haasnoot et al.[14]

QM/MD calculations were carried out for a system containing 1 molecule of L-proline or *trans*-*N*-acetyl-L-proline surrounded by TIP3P water molecules in a rectangular simulation box with the periodic boundary condition. Both the *NPT* and *NVT* calculations were undertaken, though no significant changes in endocyclic torsional curves were found between the two types of calculations. The temperature was controlled to 300 K with the Langevin algorithm, and the pressure at 1 bar was controlled using an isotropic position scaling with a 2 ps time constant. The nonbonded cutoff distance was set to 8.0 Å. After a minimization step and an equilibration QM/MD run of 40 ps, production runs were executed for 0.6−1 ns with a time step

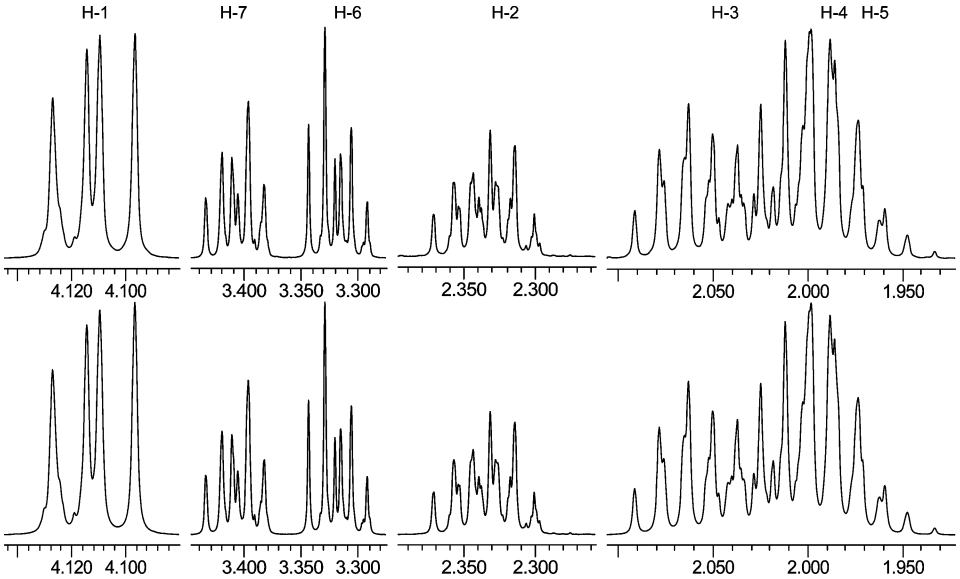

Figure 3. Experimental (top, 20 mM solution in D_2O, 298 K, nonspinning sample) and calculated (bottom) 500 MHz ^1H NMR spectra of L-proline.

of 2 fs. The mass density in the box during the production period for the *NPT* calculations was ca. 0.98 g cm^{-3}. All the QM/MD runs were performed with the PM3[33] level of theory for L-proline and its *N*-acetyl derivative and TIP3P model for water using SANDER of AMBER 9.[26] Both AM1-BCC derived charges and B3LYP/cc-pVTZ/IEFPCM calculated RESP (restrained electrostatic potential fitting) charges were used in QM/MD calculations,[34] though no significant changes in the ring conformational behavior were found on changing the charge model.[35]

Results and Discussion

Proton NMR Spectral Analysis. The published NMR data for L-proline in water reveal some inconsistencies in the reported *J*-couplings, especially in the values of the vicinal ^3J-couplings.[1,2b,36] The reason for such inconsistency is the complexity of the spectrum characteristic for a strongly coupled spin system.[10a] None of the previous analyses are complete, as no iterative fittings to experimental spectra, either by LAOCN3[10b] or full line shape[10c,d] calculations, were reported.[2b,36] These incomplete analyses of strongly coupled ^1H spectra were likely to lead to inaccurate *J*-couplings, as confirmed by our results presented below.

We employed full line shape analysis,[10c,d] which, unlike LAOCN3,[10b] avoids any peak assignments and is thus better suited for relatively large spin systems. The result of our iterative analysis is shown in Figure 3. All the characteristic spectral features caused by strong couplings (including very small peaks near 2.28 ppm) were reproduced in the calculated spectrum. The NMR parameters were determined at different temperatures and concentrations in D_2O (Table 1), as well as in CD_3OD, $CDCl_3$, and DMSO-d_6 (Supporting Information, Tables S2, S3).

Using full line shape analysis, we have also analyzed the ^1H spectrum spectrum of *N*-acetyl-L-proline (NAcPro). The analysis of the ^1H NMR spectrum of NAcPro is further complicated by the fact that signals due to both *trans*- and *cis*-rotamers about the *N*-COMe bond (Figure 4) are observed in the spectra recorded at room temperature, since the amide bond rotation is slow in the NMR time scale. As in the case of L-proline, the interconversion of C^γ-endo and C^γ-exo conformers is fast on the NMR time scale. The *trans*/*cis* ratio measured from the ^1H spectrum in D_2O at 298 K was 3.7:1. The relative orientations of the methyl groups (Figure 4) were determined using selective NOE measurements, which were additionally confirmed by the stereospecific ^5J-couplings between methyl and cyclic protons (Table 2). The spectrum due to the major *trans*-rotamer showed characteristic features of the strongly coupled spin system. Hence, the values of the *J*-couplings were determined from the full line shape analysis of the sum of ^1H spectra of the *cis*- and *trans*-rotamers (Table 2). No strong coupling effects were observed for *trans*-4-hydroxy-L-proline, and all the *J*-couplings were measured directly from ^1H NMR spectra (Table 3).

TABLE 1: Proton *J*-Couplings (in Hz) of L-Proline in D_2O Derived from Full Line Shape Analysis[a]

proton pairs	D_2O[b] 298 K	D_2O[c] 298 K	D_2O[c] 278 K	D_2O[c] 348 K	D_2O[d 36]	D_2O[e 2b]
1−2	8.81	8.81	8.81	8.79	8.4	8.7
1−3	6.61	6.61	6.65	6.53	6.2	6.2
1−4	0.06	0.06	0.07	0.07	0.0	
1−5	−0.51	−0.49	−0.50	−0.54	0.0	
1−6	−0.02	−0.02	−0.03	−0.07	0.0	
1−7	−0.39	−0.39	−0.38	−0.41	0.0	
2−3	−13.30	−13.29	−13.27	−13.32	−13.5	
2−4	7.52	7.54	7.48	7.57	7.6	7.8
2−5	6.74	6.74	6.76	6.79	5.4	7.2
2−6	0.45	0.34	0.34	0.38	0.0	
2−7	−0.46	−0.44	−0.43	−0.46	−0.4	
3−4	6.78	6.79	6.84	6.73	5.6	6.5
3−5	7.53	7.53	7.49	7.57	7.8	7.9
3−6	−0.42	−0.48	−0.48	−0.50	0.0	
3−7	0.40	0.32	0.33	0.35	0.0	
4−5	−13.23	−13.24	−13.28	−13.26	−13.0	
4−6	7.61	7.60	7.56	7.65	7.9	7.1
4−7	6.69	6.72	6.74	6.68	5.7	7.1
5−6	6.84	6.89	6.91	6.87	5.7	7.1
5−7	7.52	7.52	7.46	7.55	7.9	7.1
6−7	−11.59	−11.59	−11.58	−11.61	−11.0	

[a] For comparison, $^3J_{HH}$ couplings reported in refs 36 and 2b are also included (see also Supporting Information, Figures S1 and S2). [b] 20 mM solution, pD = 8.1 ± 0.2. [c] 320 mM solution, pD = 7.6 ± 0.2. On the basis of the iterative analysis of nine different ^1H NMR spectra recorded at three different fields (9.4, 11.7, and 16.5 T), the standard deviation is estimated to be ≤0.03 Hz for ^2J- and ^3J-couplings and ≤0.07 Hz for ^4J-couplings. [d] Values reported at pD = 7.4. The spectral parameters were determined by eye comparison of the experimental (250 MHz) and the calculated spectra.[36] [e] From the combination of a first-order multiplet analysis with a simulation of the spectrum.[2b]

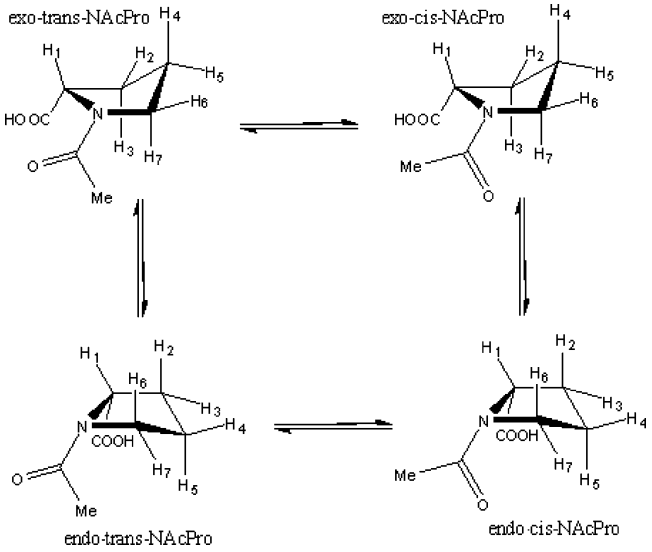

Figure 4. C^{γ}-endo/C^{γ}-exo and *cis*/*trans* equilibria in NAcPro.

TABLE 2: Experimental and Calculated *J*-Couplings (in Hz) in *cis*- and *trans*-NAcPro[a]

proton pairs	*cis*[b] J_{exp}	*cis*[c] J^{av}_{calc}	*trans*[b] J_{exp}	*trans*[c] J^{av}_{calc}
1−2	8.96	8.90	8.88	8.56
1−3	2.76	2.15	4.66	3.93
1−4	–	−0.14	−0.09	−0.09
1−5	−0.55	−0.80	−0.37	−0.81
1−6	−0.59	−0.74	−0.47	−0.80
1−7	−0.55	−0.82	−0.45	−0.78
2−3	−13.11	−12.26	−13.04	−12.31
2−4	7.01	6.46	6.99	6.21
2−5	10.90	10.01	8.68	7.61
2−6	0.41	0.06	0.23	0.13
2−7	−0.43	−0.74	−0.47	−0.68
3−4	3.37	2.65	5.62	4.85
3−5	6.79	6.42	6.83	6.41
3−6	−0.59	−0.87	−0.56	−0.79
3−7	0.59	0.35	0.39	0.21
4−5	−12.79	−11.98	−12.49	−11.74
4−6	7.38	7.16	7.38	6.76
4−7	3.54	2.50	5.29	4.29
5−6	8.95	7.94	7.25	6.29
5−7	8.41	8.21	7.74	7.24
6−7	−11.67	−11.66	−10.38	−10.08
1−Me[d]	–		0.49	
6−Me[d]	0.59		–	
7−Me[d]	0.55		–	

[a] The populations of C^{γ}-endo and C^{γ}-exo conformers determined by NMR (Table 5) were used in calculating the average *J*-couplings (J^{av}_{calc}). For the *trans*-NAcPro, the RMS deviation for 10 pairs of ^{3}J-couplings is 0.76 Hz (0.60 Hz for 21 pairs of ^{2-4}J-couplings). For the *cis*-NAcPro, the RMS deviation for 10 pairs of ^{3}J-couplings is 0.66 Hz (0.55 Hz for 21 pairs of ^{2-4}J-couplings). [b] 310 mM in D_2O, 500 MHz, 298 K. δ_H (ppm), *cis*-rotamer: 4.622 (1), 2.369 (2), 2.216 (3), 1.068 (4), 1.876 (5), 3.474 (6), 3.537 (7), and 2.017 (Me). *trans*-rotamer: 4.418 (1), 2.317 (2), 2.050 (3), 2.017 (4), 2.009 (5), 3.627 (6), 3.661 (7), and 2.117 (Me). [c] Calculations using B3LYP/6-311+G(2d,p)/IEFPCM with optimized geometries from B3LYP/6-31G(d)/IEFPCM. [d] The presence of long-range couplings (^{5}J) between methyl and cyclic protons was additionally verified using homonuclear decoupling experiments.

DFT Calculations of *J*-Couplings. In view of the recent successful applications of quantum mechanical calculations of *J*-couplings, we have carried out DFT calculations of L-prolines for further qualitative verifications of our results (Tables 2, 3, and 4). The signs and magnitudes of ^{4}J-couplings predicted using a fairly modest level of theory (DFT B3LYP/6-311+G(2d,p)/IEFPCM) were in good qualitative agreement with those determined by the full line shape analysis (Tables 2 and 4).

TABLE 3: Proton *J*-Couplings (in Hz) of *trans*-4-Hydroxy-L-proline in D_2O[a]

proton pairs	J_{exp}[b] 298 K	J_{exp}[c] 278 K	J_{exp}[e] 298 K	J_{exp}[d] 348 K	J^{exo}_{calc}[f] C^{γ}−exo, $^{\gamma}$E
1−2	7.97	7.92	7.97	8.04	8.82
1−3	10.23	10.41	10.26	9.71	8.23
1−5	−0.69	−0.73	−0.69	−0.67	−0.97
1−6	–	–	–	–	−0.08
1−7	−0.34	−0.30	−0.32	−0.27	−0.68
2−3	−14.11	−14.07	−14.08	−14.10	−13.47
2−5	1.70	1.54	1.69	2.01	0.63
2−6	2.05	2.09	2.00	1.93	1.96
2−7	–	–	–	–	0.29
3−5	4.37	4.26	4.37	4.65	4.04
3−6	–	–	–	–	−0.15
3−7	0.47	0.45	0.48	0.47	0.66
5−6	1.40	1.23	1.41	1.77	0.43
5−7	3.82	3.69	3.80	4.14	2.14
6−7	−12.61	−12.57	−12.60	−12.63	−11.76

[a] On the assumption of the sole predominance of the C^{γ}-exo conformer, the RMS deviation for 6 pairs of ^{3}J-couplings at 278 K is 1.26 Hz (0.95 Hz for 12 pairs of ^{2-4}J-couplings). [b] 32 mM (pD 7.5 ± 0.2), δ_H (ppm): 4.334 (1), 2.422 (2), 2.147 (3), 4.657 (5), 3.347 (6), 3.472 (7). [c] 870 mM, δ_H (ppm): 4.343 (1), 2.431 (2), 2.140 (3), 4.665 (5), 3.356 (6), 3.466 (7). [d] 870 mM, δ_H (ppm): 4.336 (1), 2.418 (2), 2.145 (3), 4.654 (5), 3.352 (6), 3.473 (7). [e] 870 mM, δ_H (ppm): 4.331 (1), 2.402 (2), 2.180 (3), 4.642 (5), 3.354 (6), 3.505 (7). [f] B3LYP/6-311+G(2d,p)/IEFPCM, the geometry from B3LYP/6-31G(d)/IEFPCM.

TABLE 4: Calculated *J*-Couplings in L-Proline[a]

proton pairs	J_{exp}[b]	J^{av}_{calc}[c]	J^{av}_{calc}[d]	J^{av}_{calc}[e]	J^{av}_{calc}[f]
1−2	8.81	7.65	9.04	8.74	8.57
1−3	6.61	5.82	4.80	5.57	5.56
1−4	0.06		−0.06	−0.04	−0.07
1−5	−0.49		−0.84	−0.75	−0.76
1−6	−0.02		−0.22	−0.21	−0.24
1−7	−0.39		−0.74	−0.65	−0.73
2−3	−13.29		−12.55	−11.87	−12.03
2−4	7.54	6.59	6.37	6.21	6.60
2−5	6.74	6.65	6.13	6.24	6.09
2−6	0.34		0.38	0.39	0.32
2−7	−0.44		−0.64	−0.62	−0.73
3−4	6.79	6.67	5.95	6.00	5.92
3−5	7.53	6.62	6.24	6.11	6.63
3−6	−0.48		−0.71	−0.64	−0.71
3−7	0.32		0.23	0.28	0.23
4−5	−13.24		−12.52	−11.93	−12.5
4−6	7.60	6.25	6.27	6.50	6.73
4−7	6.72	6.33	6.17	6.14	5.98
5−6	6.89	6.33	6.12	6.19	6.12
5−7	7.52	6.26	6.13	6.28	6.23
6−7	−11.59		−10.99	−10.46	−11.66
RMS(^{3}J)		0.87	1.10	0.97	0.87
RMS(^{2-4}J)			0.81	0.83	0.70

[a] The optimized geometries of C^{γ}-endo and C^{γ}-exo conformations by the DFT calculations were $_{\gamma}$E and $^{\gamma}$E, respectively (Table 6). Equal populations of C^{γ}-endo and C^{γ}-exo conformations were assumed in calculating averaged *J*-couplings (J^{av}_{calc}). [b] 320 mM solution, pD = 7.6 ± 0.2. [c] Calculations using dihedral angles from the B3LYP/6-311++G(2df,2pd)/IEFPCM optimized geometries and eqs 8C and 8D by Haasnoot et al.[14] [d] Calculations using B3LYP/6-311+G(2d,p)/IEFPCM and optimized geometries from B3LYP/6-31G(d)/IEFPCM. [e] Calculations using B3LYP/6-311++G(2df,2pd)/IEFPCM and optimized geometries at the same level of theory. [f] Calculations using B3LYP/6-311+G(2d,p)/IEFPCM. The NMR predicted dihedral angles χ_1−χ_5 (Table 6) were fixed in DFT B3LYP/6-31G(d)/IEFPCM geometry optimizations.

TABLE 5: Geometry and Conformational Populations of L-Proline at 298 K Derived from Least-Squares Fittings of $^3J_{HH}$-Couplings[a]

C$^\gamma$−endo/C$^\gamma$−exo		P^{endo}/P^{exo} (°)	χ_m (°)	x^{endo}	RMS (Hz)
L-proline in D_2O	$_\gamma T^\delta - _\gamma E/_\beta T^\gamma$	206/3	39	0.50	0.50
L-proline in CD_3OD	$_\gamma T^\delta - _\gamma E/_\beta T^\gamma$	205/3	39	0.52	0.46
L-proline in $CDCl_3$	$_\gamma E/^\gamma E$	200/17	42	0.55	0.55
L-proline in DMSO−d_6	$_\gamma E/_\beta T^\gamma$	201/5	39	0.59	0.40
cis−NAcPro in D_2O	$_\gamma T^\beta/^\gamma E$	180/23	40	0.80	0.55
trans−NAcPro in D_2O	$_\gamma T^\beta/^\gamma E$	185/14	40	0.61	0.49

[a] The least-squares fitting errors were ± 1.0° for P, ±0.3° for χ_m, and ± 0.003 for x^{endo}.

The results also show that the DFT-predicted *J*-couplings can be useful as starting guess values at the spectral simulation stage of the strongly coupled spin systems.

The combination of NMR-predicted populations (see below) with the DFT B3LYP/6-311+G(2d,p)/IEFPCM calculations proved successful, resulting in RMS of 0.7−1.3 Hz for $^3J_{HH}$-couplings (Tables 2−4). In the case of L-proline, the performance of a more CPU-demanding B3LYP/6-311++G(2df,2pd)/IEFPCM calculation resulted in only small improvement (Table 4), while the absolute values of the predicted geminal couplings were significantly less than those measured experimentally. On using the DFT B3LYP optimized geometries of L-proline, the performance of the empirically derived Karplus-type equations by Haasnoot et al.[14] was found to be better than those of B3LYP *J*-calculations (Table 4). Additionally, the dihedral angles derived from the least-squares fittings of ^3J-couplings (see below) via Karplus-type equations by Haasnoot et al.[14] were used. These were fixed in the DFT geometry optimizations, and the resulting geometries were then used in the DFT calculations of the *J*-couplings. The calculated values in this way (Table 4, last column) were in better agreement with the experimentally determined *J* values than those from the unrestricted geometry optimization (Table 4, column 4).

Conformational Analysis Using Proton NMR ^3J-Couplings. The best part of the literature on experimental and computational studies of L-proline and related derivatives relies on the conformational geometries and populations derived by Haasnoot et al.[1] They employed least-squares fittings of ^3J-couplings using a simple two-site equilibrium model between C$^\gamma$-endo and C$^\gamma$-exo conformers (Figure 1) and Karplus-type equations.[14] However, the experimental values of ^3J-couplings used in their fittings were derived from incomplete spectral analysis[36] and are significantly different from those obtained by us from full line shape analysis (Table 1). Thus, the reliability of the results for L-proline can be questioned. Note that the B3LYP/COSMO calculated geometries were assumed in a recent analysis of NMR data to estimate the conformer populations of L-proline in water.[2b] However, the correctness of such an assumption is not obvious, since, by their own admission,[2b] the B3LYP/COSMO model may not be adequate for accurate description of strong interactions between the solvent and the polar groups of the solute.

In view of the above uncertainties, we reexamine the conformational geometries and populations of L-proline in water using accurate values of ^3J-couplings derived from the full line shape analysis. As in the previous work,[1] we intend to derive both the conformational populations and geometries from the ^3J-couplings. For ease of comparison, we use the original conformational notation for L-prolines.[1] In particular, E and T letters are used to denote envelope and twist conformations, with a superscript (subscript) indicating a proline ring atom above (below) the ring. The downward orientation of the CO_2 group is used as a reference view, and the exo- and endo-orientaions of the ring carbons are defined relative to CO_2 (Figure 1). For endocyclic torsional angles, we use the conventional χ notation

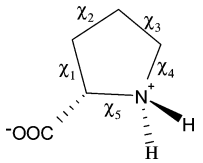

In line with the previous studies, we use the pseudorotation phase angle, P, and amplitude, χ_m, for the description of the pyrrolidine ring conformations. The value of P identifies a given ring conformation on the pseudorotation circle, whereas χ_m is the maximum value attained by the endocyclic torsional angles $\chi_1-\chi_5$. For the calculations of $\chi_1-\chi_5$ or for the backward calculations of P and χ_m, we used equations by Altona−Sundaralingam[37] or by Westhof−Sundaralingam.[38] Calculations by both sets of equations resulted in similar values within rounding errors. Note that 180° is added to the calculated P value if $\chi_2 < 0$.

The results of our analysis using a least-squares fitting similar to that described previously,[1] but based on the simulated annealing algorithm,[13] are summarized in Table 5. As before, we have considered a simple two-site conformational equilibrium between C$^\gamma$-endo and C$^\gamma$-exo conformers (see below comparisons with DFT calculations[2b] and MD simulations). Further analysis involving Gaussian distributions of P and χ_m or the increase of the number of conformers in equilibrium (up to eight-site model) did not achieve improvements in RMS of ^3J-fittings and effectively converged to the solution found for the two-site C$^\gamma$-endo/C$^\gamma$-exo equilibrium model. A consideration of $\chi_m^{endo} \neq \chi_m^{exo}$ and $\chi_m^{endo} = \chi_m^{exo}$ cases showed insignificant or no changes in RMS; hence, the results for $\chi_m^{endo} = \chi_m^{exo}$ were used.

The predicted populations of conformers (x^{endo} and $x^{exo} = 1 - x^{endo}$) confirmed that the pyrrolidine ring is evenly distributed between two conformers in water, in agreement with the previous results,[1,2b] despite the apparent asymmetry of the structure due to the presence of the carboxylic group in the α-position. A slight preference of the C$^\gamma$-endo form, however, is observed on changing the solvent from D_2O to CD_3OD ($x^{endo} = 0.52$). From further measurements in other solvents, the x^{endo} values were 0.55 in $CDCl_3$ and 0.59 in DMSO-d_6. With regard to the ring geometries deduced from NMR, they showed better agreement with the DFT optimized geometries (Table 6), as well as with the gas-phase geometry of neutral L-proline,[2a] but not with the single-crystal structure of L-proline[9a] or DL-proline.[9c]

Only very small changes of ^3J-couplings (<2%) were observed in L-proline in D_2O on temperature variations between 278 and 348 K. On using a combined least-squares fitting of 30 ^3J-couplings at three different values of T (Table 1), the best fit values were $P^{endo} = 206°$, $P^{exo} = 3°$, $\chi_m = 39°$, $x^{endo}(278K) = 0.495$, $x^{endo}(298K) = 0.496$, and $x^{endo}(348K) = 0.499$ (RMS = 0.53 Hz), in agreement with the best-fit values obtained from

TABLE 6: Pseudorotation Parameters and Torsional Angles in L-Proline

	method	conformation	P (°)	χ_m (°)	χ_1 (°)	χ_2 (°)	χ_3 (°)	χ_4 (°)	χ_5 (°)
single crystal	X−ray, L-proline[9a]	C^γ−endo, ${}_\gamma T^\beta$	179	41	34	−41	34	−12	−14
in D_2O	NMR	C^γ−endo, ${}_\gamma T^\delta$−${}_\gamma E$	206	39	19	−35	39	−27	5
in CD_3OD	NMR	C^γ−endo, ${}_\gamma T^\delta$−${}_\gamma E$	205	39	19	−36	39	−27	5
zwitterion	B3LYP/6−31G(d)/ IEFPCM	C^γ−endo, ${}_\gamma E$	193	41	27	−40	37	−21	−4
zwitterion	B3LYP/6−311++G(2df,2pd)/ IEFPCM	C^γ−endo, ${}_\gamma E$	195	40	25	−39	37	−22	−2
zwitterion	B3LYP/cc−pvTZ/IEFPCM	C^γ−endo, ${}_\gamma E$	194	40	26	−39	37	−21	−3
in D_2O	NMR	C^γ−exo, ${}_\beta T^\gamma$	3	39	−30	39	−33	14	10
in CD_3OD	NMR	C^γ−exo, ${}_\beta T^\gamma$	4	39	−31	39	−33	14	11
zwitterion	B3LYP/6−31G(d)/IEFPCM	C^γ−exo, ${}^\gamma E$	23	40	−21	36	−38	26	−3
zwitterion	B3LYP/6−311++G(2df,2pd)/ IEFPCM	C^γ−exo, ${}^\gamma E$	13	40	−27	39	−37	21	4
zwitterion	B3LYP/cc−pvTZ/IEFPCM	C^γ−exo, ${}^\gamma E$	12	40	−27	39	−37	20	4

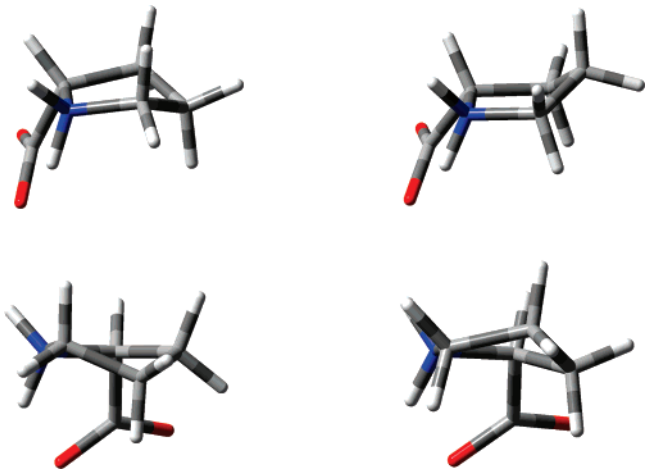

Figure 5. The NMR predicted ring geometries for C^γ-endo (left) and C^γ-exo (right) conformers of L-proline. The same conformation from two different view angles is shown in each column.

fitting of 10 ^3J-couplings at 298 K (Table 5). The very small increase of x^{endo} with temperature is on the order of the least-squares fitting error involved (±0.003).

To summarize the results for L-proline, the NMR-predicted geometry of the C^γ-endo conformer in water can be identified as intermediate between ${}_\gamma T^\delta$ and ${}_\gamma E$, and that of the C^γ-exo conformer as ${}_\beta T^\gamma$ (Figure 5). For comparison, previously found conformations were ${}_\gamma E$ (C^γ-endo) and ${}_\beta T^\gamma$ (C^γ-exo),[1] i.e., although based on highly inaccurate ^3J-values, the geometries found by Haasnoot et al. are not far from that found by us. Note that the E-conformers used in the recent publication are not from NMR, but from B3LYP/COSMO calculations.[2b]

Using similar full line shape analysis and least-squares ^3J-fittings, we have also studied *cis*- and *trans*-*N*-acetyl-L-prolines. Both rotamers showed major changes in the populations and geometries of the conformers (Table 5) compared to L-Lproline. We note that neither *cis*- nor *trans*-NAcPro was analyzed previously due to the complexity of their NMR spectra. The study of $NAcProNH_2$ was reported, but only for the *cis*-rotamer.[1] Comparison of the NMR-derived conformational geometries with those predicted by DFT (Table 7) showed significantly better agreement for *cis*- and *trans*-NAcPro (with no formal charge on the pyrrolidine nitrogen) compared to zwitterionic L-proline (Table 6).

In comparison to L-proline, *J*-couplings of *trans*-4-hydroxy-L-proline in D_2O showed a more significant temperature dependence. Previously, *trans*-4-hydroxy-L-proline was shown to adopt exclusively a C^γ-exo conformation in D_2O at room temperature.[1] While the preference of the C^γ-exo geometry is supported by the observed *J*-couplings (e.g., very small values of ^3J-couplings for proton torsional angles near 90° or a W-type ^4J-coupling of ca. 2 Hz between protons 2 and 6 (Table 3)), its exclusiveness nevertheless may require reconsideration in view of the observed temperature dependence of *J*-couplings. From a combined least-squares fitting of 60 ^3J-couplings at 10 different temperatures under the two-site equilibrium model (Supporting Information Table S4), the best fit value for the population of the major conformer with $P = 17°/\chi_m = 42°$ (${}^\gamma E$) was 1 at 278, 288, and 298 K; 0.99 at 308, 318, and 328 K; 0.97 at 338 K; 0.95 at 348 K; 0.94 at 358 and 368 K (RMS = 0.28 Hz). The best fit pseudorotation parameters of the major conformer are in good agreement with those from the neutron diffraction studies ($P = 23°/\chi_m = 35°$ at room temperature).[9d] For the minor conformer, the predicted values were $P = 241°/\chi_m = 43°$ (${}^\delta E$), although these values of pseudorotation parameters are likely to be less accurate due to very low population of the second conformer.

MD Simulations. The main disadvantage of spectroscopic techniques, including NMR, is that they do not provide a direct visual presentation of a process of conformational changes, but rather rely on the model dependent analysis of the dynamically averaged parameters. In principle, MD simulations are capable of providing such information at an atomistic level. The drawback of MD, however, is that it is a "thought experiment", optimized as much as possible to lead to a realistic result and yet without confidence of experiment. Thus, a combined NMR/MD approach is likely to lead to a more accurate view of fast conformational processes.

Here, we use MD simulations primarily for the purpose of verification of whether the two-site C^γ-endo/C^γ-exo exchange model used in the analysis of the NMR data is also in agreement with the predictions from independent and unrestricted MD calculations. Due to the intrinsic limitations of both methods, the NMR/MD comparison, as well as DFT and X-ray geometries are also used for "backward" verification of the MD performance. On a particular note, while the MD studies have mainly focused on acyclic peptide conformations, the behavior of flexible rings under MD conditions is less well known. Thus, we examine the performance of various force fields used in MD simulations for predicting the preferred ring conformations of L-proline and *trans*-*N*-acetyl-L-proline.

The results using GROMOS,[18] AMBER[22] and OPLS-AA[20] force fields, as well as QM/MD simulations, are detailed in Table 8. A zwitterionic L-proline molecule surrounded by >800 water molecules in a periodic box was used in the simulations. In the hybrid QM/MD calculations, the solute's intramolecular energy and forces were calculated using the PM3 method[33] and the water molecules were represented by the TIP3P model.[21]

Overall, none of the classical MD simulations of L-proline in water were able to reproduce the conformational geometries and populations derived from the NMR analysis accurately. The predicted ring conformations and their populations were also in disagreement among the force fields used. In comparison to AMBER and OPLS-AA, the GROMOS force field performed

TABLE 7: Pseudorotation Parameters and Torsional Angles in *N*-Acetyl-L-prolines[a]

	method	conformation	P (°)	χ_m(°)	χ_1(°)	χ_2(°)	χ_3(°)	χ_4(°)	χ_5(°)
cis, D_2O	NMR	C^γ−endo, ${}_\gamma T^\beta$	180	40	33	−40	33	−12	−13
cis, calc	DFT	C^γ−endo, ${}^\beta E-{}_\gamma T^\beta$	171	38	33	−37	27	−6	−17
cis, D_2O	NMR	C^γ−exo, ${}^\gamma E$	23	40	−21	37	−39	27	−4
cis, calc	DFT	C^γ−exo, ${}^\gamma E$	18	38	−22	36	−35	22	0
trans, D_2O	NMR	C^γ−endo, ${}_\gamma T^\beta$	185	40	31	−40	34	−16	−9
trans, calc	DFT	C^γ−endo, ${}_\gamma T^\beta$	182	37	29	−37	31	−13	−11
trans, D_2O	NMR	C^γ−exo, ${}^\gamma E$	14	40	−26	39	−37	22	3
trans, calc	DFT	C^γ−exo, ${}^\gamma E$	10	38	−26	37	−34	18	5

[a] The DFT geometry optimizations of neutral NAcPro rotamers employed B3LYP/6-31G(d)/IEFPCM level of theory.

TABLE 8: Conformational Populations and Geometries of L-Proline and *trans*-NAcPro in Water from NMR and MD[a]

	method	C^γ−endo/C^γ−exo	P^{endo}/χ_m (°)	P^{exo}/χ_m (°)	x^{endo}	RMS (Hz)	RMS_{HH} (Hz)
L-proline	NMR	${}_\gamma E-{}_\gamma T^\delta/{}_\beta T^\gamma$	206/39	3/39	0.50	0.50	–
(zwitterion)	53a6	${}_\gamma T^\beta/{}_\beta E-{}_\beta T^\gamma$	179/40	−9/40	0.32	1.50	–
	GAFF	${}_N E$	*b*	*c*	*c*	1.84	1.77
	OPLS−AA	${}^\beta E-\gamma T^\beta/{}_\beta E-{}_\beta T^\gamma$	171/31	−13/31	0.75	2.08	1.99
	PM3	${}_\gamma E-{}_\gamma T^\delta/{}_\beta T^\gamma-{}^\gamma E$	∼210/28	∼8/28	∼0.45	1.83	1.91
trans−NAcPro	NMR	${}_\gamma T^\beta/{}^\gamma E$	185/40	14/40	0.61	0.49	–
	53a6	${}_\gamma T^\beta/{}_\beta T^\gamma-{}^\gamma E$	179/39	6/39	0.53	1.06	–
	53a6[d]	${}_\gamma T^\beta/{}_\beta T^\gamma-{}^\gamma E$	179/39	8/39	0.53	1.04	–
	GAFF	${}_\gamma T^\beta/{}_\beta T^\gamma$	178/31	4/31	0.45	1.82	1.81
	AMBER94[d]	${}_\gamma T^\beta/{}_\beta T^\gamma-{}^\gamma E$	178/36	7/36	0.59	1.10	0.80
	AMBER99[d]	${}_\gamma T^\beta/{}_\beta T^\gamma-{}^\gamma E$	178/35	6/35	0.57	1.21	0.92
	AMBER03[d]	${}_\gamma T^\beta/{}_\beta T^\gamma-{}^\gamma E$	177/36	10/36	0.65	1.09	0.76
	OPLS−AA	${}^\beta E-{}_\gamma T^\beta/{}_\beta T^\gamma$	170/32	−5/32	0.97	2.36	2.28
	PM3	${}^\beta E-{}_\gamma T^\beta/{}_\delta T^\gamma$	∼170/25	∼40/25	∼0.6	2.21	2.57

[a] As the cyclic ^1H positions are not available from GROMOS, P and χ_m values were calculated for each set of $\chi_1-\chi_5$, which then were used for the calculation of $^1H-{}^1H$ dihedral angles via eq 3.[1] The RMS values for these calculations are listed under "RMS" and are used for comparisons. The RMS_{HH} values were also calculated, where ^1H positions were available from MD trajectories. [b] Only the major conformer with $P = -85°$ and $\chi_m = 42°$ was identified. [c] Not measured, due to the complex shape of the calculated distribution curves. [d] A CO_2^- terminated *trans*-NAcPro with a Na^+ cation added for neutralization was used.

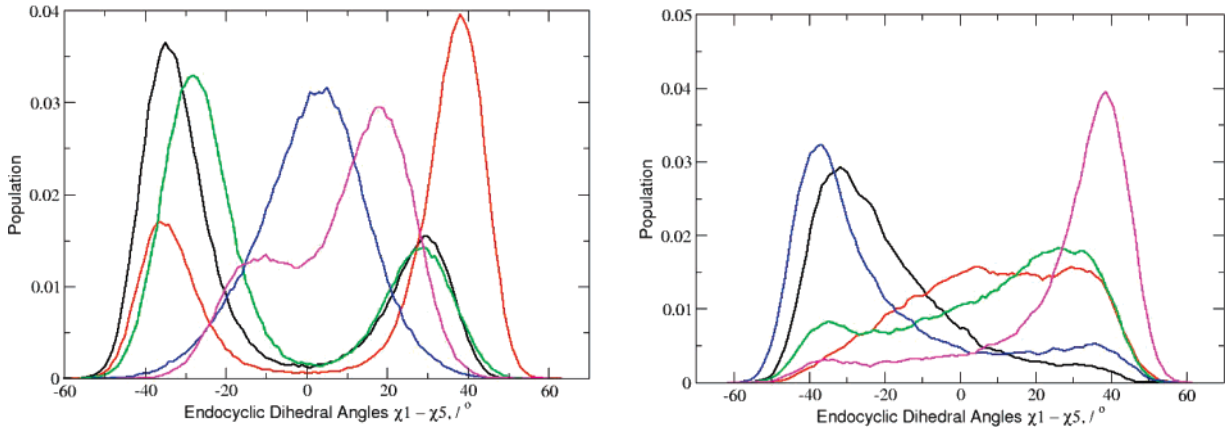

Figure 6. Endocyclic torsional angle distributions in L-proline in water from MD simulations using GROMOS 53a6 (left)[18] and GAFF (right).[24] Colors used: χ_1 (black), χ_2 (red), χ_3 (green), χ_4 (blue), and χ_5 (magenta).

relatively better in predicting the χ_m value, which was in good agreement with the NMR, X-ray diffraction, and DFT results (Table 6). The value of the pseudorotation phase angle P predicted by GROMOS for the minor C^γ-endo conformer was the same as that from the X-ray diffraction, but in disagreement with NMR. The results of both the GROMOS and OPLS-AA calculations were in agreement with a two-site equilibrium model, although the populations and geometries of conformers were significantly different from those predicted by NMR. The interpretation of the torsional curves predicted by generalized AMBER force field (GAFF)[24] was less straightforward, although judging by the appearance of some of the χ-curves, there may be more than two conformations in equilibrium (Figure 6). The PM3 QM/MD approach was able to reproduce approximately equal populations of the two L-proline conformations in water (Figure 7). The predicted pseudorotation phase angles for the C^γ-endo and C^γ-exo conformers were in good agreement with those from NMR, although their preference was not significant, and the endocyclic torsions predicted were significantly smaller than those from NMR, X-ray diffraction, and DFT calculations (Table 6, compare χ_m values), leading to relatively high RMS for calculated $^3J_{HH}$-couplings.

The poor disagreement between MD and NMR results may be due to the zwitterionic nature of L-proline, which is presumably not accounted for adequately in force field parametrizations. In the case of *N*-capped *trans*-NAcPro with no formal charge on the pyrrolidine nitrogen, MD simulations in water led to a nearly quantitative agreement with NMR results on using GROMOS 53a6 and various AMBER force fields (Figure 8), with the RMS deviation of ca. 1 Hz for $^3J_{exp}$ vs $^3J_{calc}$. The results by the OPLS-AA force field or QM/MD approach with RMS > 2 Hz, however, were less satisfactory.

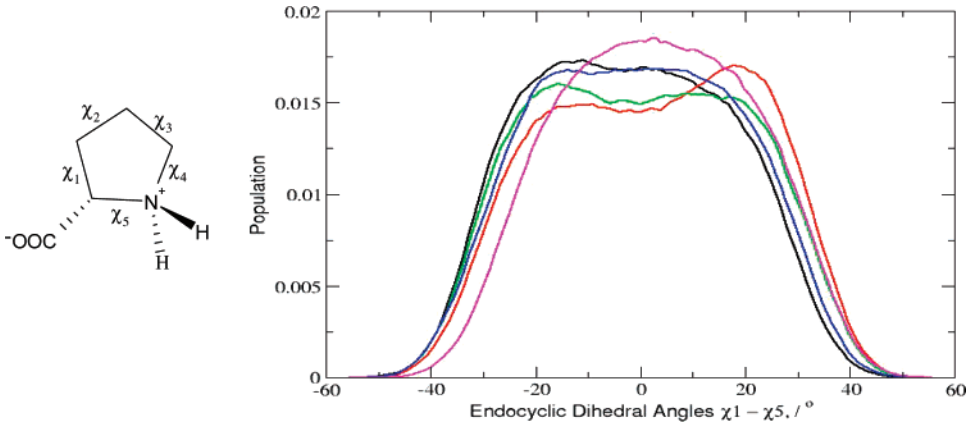

Figure 7. Endocyclic torsional angle distributions in L-proline from a 0.98 ns QM/MD simulation with a PM3 level of theory for L-proline. Colors used: χ_1 (black), χ_2 (red), χ_3 (green), χ_4 (blue), and χ_5 (magenta).

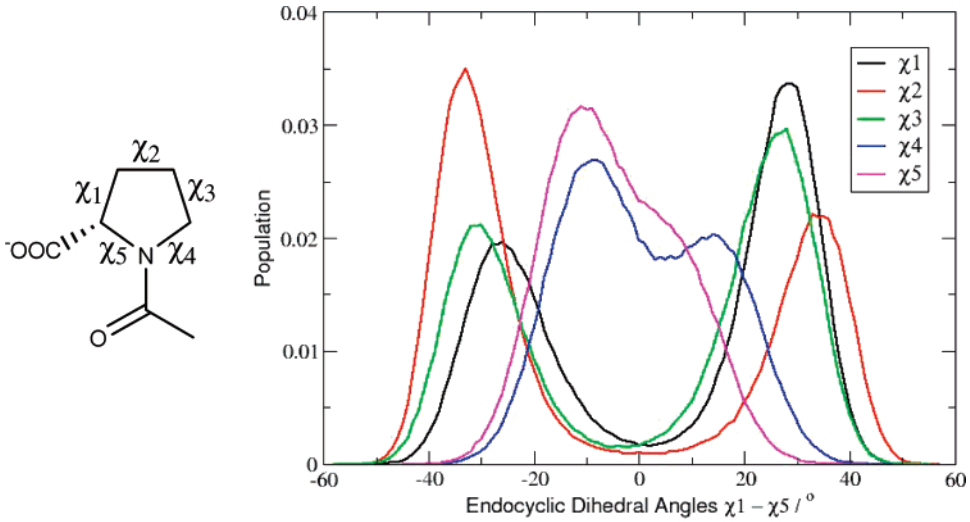

Figure 8. Endocyclic torsional angle distributions in *trans*-NAcPro from a 10 ns MD simulation using AMBER94.[22a] A CO_2^--terminated *trans*-NAcPro was used with a Na^+ cation added for neutralization.

As in the case of L-proline, significantly flattened ring geometries with $\chi_m = 32°$ for OPLS-AA and $\chi_m = 25°$ for PM3 QM/MD were predicted compared to other force fields, as well as NMR analysis and DFT calculations (Table 7). We note that the relatively small values of the endocyclic torsions predicted by PM3 is also in agreement with the previous results reported for *N*-acetyl-L-proline amide by Ramek et al.[39]

In summary, a diverse performance of MD and QM/MD calculations makes their solitary use a somewhat less confident approach for the analysis of highly flexible pyrrolidine rings in L-prolines. Nevertheless, the results of MD simulations were mostly in favor of a two-site equilibrium model used in our NMR analysis, especially in the case of NAcPro. The presence of the two distinct but equally populated flexible foRMS of zwitterionic L-proline in aqueous solution is also in agreement with the recent results of the potential energy surface calculations using B3LYP/COSMO and DFT-assisted analysis of Raman spectra.[2b]

Acknowledgment. We are grateful for the provision of studentship from the Royal Institution (D.C.M.). We thank Laure Jerome and Sandra Luengo-Arratta (Department of Chemistry, University College London) for their help with pH measurements and sample preparations and Dr. Rainer Kümmerle (Bruker Biospin IG, Fällanden, Switzerland) for recording ^{1}H NMR spectrum of L-proline on AVANCE700.

Supporting Information Available: Further results of NMR measurements, DFT, and MD calculations. This material is available free of charge via the Internet at http://pubs.acs.org.

References and Notes

(1) Haasnoot, C. A. G.; DeLeeuw, F. A. A. M.; DeLeew, H. P. M.; Altona, C. *Biopolymers* **1981**, *20*, 1211.

(2) (a) Lesarri, A.; Mata, S.; Cocinero, E. J.; Blanco, S.; López, J. C.; Alonso, J. L. *Angew. Chem., Int. Ed.* **2002**, *41*, 4673. (b) Kapitán, J.; Baumruk, V.; Kopecký, V.; Pohl, R.; Bouř, P. *J. Am. Chem. Soc.* **2006**, *128*, 13451. (c) Allen, W. D.; Czinki, E.; Császár, G. A. *Chem.—Eur. J.* **2004**, *10*, 4512. (d) Cappelli, C.; Monti, S.; Rizzo, R. *Int. J. Quantum Chem.* **2005**, *104*, 744. (e) Kang, Y. K. *J. Phys. Chem. B* **2004**, *108*, 5463. (f) Pecul, M.; Ruud, K.; Rizzo, A.; Helgaker, T. *J. Phys. Chem. A* **2004**, *108*, 4269. (g) Sahai, M. A.; Kehoe, T. A. K.; Koo, J. C. P.; Setiadi, D. H.; Chass, G. A.; Viskolcz, B.; Penke, B.; Pai, E. F.; Csizmadia, I. G. *J. Phys. Chem. A* **2005**, *109*, 2660. (h) Lesarri, A.; Cocinero, E. J.; Lopez, J. C.; Alonso, J. L. *J. Am. Chem. Soc.* **2005**, *127*, 2572. (i) Taylor, C. M.; Hardre, R.; Edwards, P. J. B. *J. Org. Chem.* **2005**, *70*, 1306.

(3) (a) Lanza, G.; Salvi, A. M.; Tamburro, A. M. *J. Mol. Struct.* **2007**, *812*, 25. (b) Kapitán, J.; Baumruk, V.; Kopecký, V.; Bouř, P. *J. Phys. Chem. A* **2006**, *110*, 4689. (c) Bouř, P.; Budesinsky, M.; Spirko, V.; Kapitán, J.; Sebestik, J.; Sychrovsky, V. *J. Am. Chem. Soc.* **2005**, *127*, 17079. (d) Jalkanen, K. J.; Elstner, M.; Suhai, S. *J. Mol. Struct.* **2004**, *675*, 61. (e) Parthasarathi, R.; Madhan, B.; Subramanian, V.; Ramasami, T. *Theor. Chem. Acc.* **2003**, *110*, 19.

(4) (a) Brunne, R. M.; van Gunsteren, W. F.; Brüschweiler, R.; Ernst, R. R. *J. Am. Chem. Soc.* **1993**, *115*, 4764. (b) Schmidt, J. M.; Brüschweiler, R.; Ernst, R. R.; Dunbrack, R. L.; Joseph, D.; Karplus, M. *J. Am. Chem. Soc.* **1993**, *115*, 8747. (c) Hu, H.; Elstner, M.; Hermans, J. *Proteins* **2003**, *50*, 451. (d) Mu, Y.; Kosov, D. S.; Stock, G. *J. Phys. Chem. B* **2003**, *107*,

5064. (e) Hugosson, H. W.; Laio, A.; Maurer, P.; Rothlisberger, U. *J. Comput. Chem.* **2006**, *27*, 672. (f) Graf, J.; Nguyen, P. H.; Stock, G.; Schwalbe, H. *J. Am. Chem. Soc.* **2007**, *129*, 1179. (g) Scheraga, H. A.; Khalili, M.; Liwo, A. *Annu. Rev. Phys. Chem.* **2007**, *58*, 57.

(5) (a) Mooney, S. D.; Kollman, P. A.; Klein, T. E. *Biopolymers* **2002**, *64*, 63. (b) Park, S.; Radmer, R. J.; Klein, T. E.; Pande, V. S. *J. Comput. Chem.* **2005**, *26*, 1612.

(6) (a) Bronco, S.; Cappelli, C.; Monti, S. *J. Phys. Chem. B* **2004**, *108*, 10101. (b) Monti, S.; Bronco, S.; Cappelli, C. *J. Phys. Chem. B* **2005**, *109*, 11389. (c) Berisio, R.; Vitagliano, L.; Mazzarella, L.; Zagari, A. *Protein Sci.* **2002**, *11*, 262. (d) Kramer, R. Z.; Bella, J.; Mayville, P.; Brodsky, B.; Berman, H. M. *Nat. Struct. Biol.* **1999**, *6*, 454. (e) Melacini, G.; Bonvin, A. M. J. J.; Goodman, M.; Boelens, R.; Kaptein, R. *J. Mol. Biol.* **2000**, *300*, 1041. (f) Handgraaf, J.-W.; Zerbetto, F. *Proteins* **2006**, *64*, 711.

(7) (a) Sone, M.; Yoshimizu, H.; Kurosu, H.; Ando, I. *J. Mol. Struct.* **1994**, *301*, 227. (b) Saitô, H.; Yokoi, M. *J. Biochem.* **1992**, *111*, 376.

(8) (a) Dorman, D. E.; Bovey, F. A. *J. Org. Chem.* **1973**, *38*, 2379. (b) Siemion, I. Z.; Wieland, T.; Pook, K.-H. *Angew. Chem.* **1975**, *87*, 702. (c) Vitagliano, L.; Berisio, R.; Mastrangelo, A.; Mazzarella, L.; Zagari, A. *Protein Sci.* **2001**, *10*, 2627. (d) Pal, D.; Chakrabarti, P. *J. Mol. Biol.* **1999**, *294*, 271. (e) Shoulders, M. D.; Hodges, J. A.; Raines, R. T. *J. Am. Chem. Soc.* **2006**, *128*, 8112.

(9) (a) Kayushina, K. L.; Vainshtein, B. K. *Sov. Phys. Crystallogr.* **1965**, *10*, 698. (b) Janczak, J.; Luger, P. *Acta Crystallogr., Sect. C* **1997**, *53*, 1954. (c) Myung, S.; Pink, M.; Baik, M.-H.; Clemmer, D. E. *Acta Crystallogr., Sect.C* **2005**, *61*, 506. (d) Koetzle, T. F.; Lehmann, M. S.; Hamilton, W. C. *Acta Crystallogr., Sect. B* **1973**, *29*, 231.

(10) (a) Günther, H. *NMR Spectroscopy*, 2nd ed.; Wiley: Weinheim, 1995. (b) Castellano, S. M.; Bothner-By, A. A. *J. Chem. Phys.* **1964**, *41*, 3863.(c) Stephenson, D.; Binsch, G. *J. Magn. Reson.* **1980**, *37*, 395. (d) Hägele, G.; Engelhardt, M.; Boenigk, M. *Simulation und automatisierte Analyse von Kernresonanzspektren*; VCH: Weinheim, 1987.

(11) Mikkelsen, K.; Nielsen, S. O. *J. Phys. Chem.* **1960**, *64*, 632.

(12) *gNMR*, version 5.0.6; NMR Simulation Program, Budzelaar PHM, 2006.

(13) Press, W. H.; Flannery, B. P.; Teukolsky, S. A. *Numerical Recipes in FORTRAN: the Art of Scientific Computing*; Cambridge University Press: Cambridge, 1992.

(14) Haasnoot, C. A. G.; DeLeeuw, F. A. A. M.; Altona, C. *Tetrahedron* **1980**, *36*, 2783.

(15) Karplus, M. *J. Am. Chem. Soc.* **1963**, *85*, 2870.

(16) Frisch, M. J.; Trucks, G. W.; Schlegel, H. B.; Scuseria, G. E.; Robb, M. A.; Cheeseman, J. R.; Montgomery, J. A., Jr.; Vreven, T.; Kudin, K. N.; Burant, J. C.; Millam, J. M.; Iyengar, S. S.; Tomasi, J.; Barone, V.; Mennucci, B.; Cossi, M.; Scalmani, G.; Rega, N.; Petersson, G. A.; Nakatsuji, H.; Hada, M.; Ehara, M.; Toyota, K.; Fukuda, R.; Hasegawa, J.; Ishida, M.; Nakajima, T.; Honda, Y.; Kitao, O.; Nakai, H.; Klene, M.; Li, X.; Knox, J. E.; Hratchian, H. P.; Cross, J. B.; Bakken, V.; Adamo, C.; Jaramillo, J.; Gomperts, R.; Stratmann, R. E.; Yazyev, O.; Austin, A. J.; Cammi, R.; Pomelli, C.; Ochterski, J. W.; Ayala, P. Y.; Morokuma, K.; Voth, G. A.; Salvador, P.; Dannenberg, J. J.; Zakrzewski, V. G.; Dapprich, S.; Daniels, A. D.; Strain, M. C.; Farkas, O.; Malick, D. K.; Rabuck, A. D.; Raghavachari, K.; Foresman, J. B.; Ortiz, J. V.; Cui, Q.; Baboul, A. G.; Clifford, S.; Cioslowski, J.; Stefanov, B. B.; Liu, G.; Liashenko, A.; Piskorz, P.; Komaromi, I.; Martin, R. L.; Fox, D. J.; Keith, T.; Al-Laham, M. A.; Peng, C. Y.; Nanayakkara, A.; Challacombe, M.; Gill, P. M. W.; Johnson, B.; Chen, W.; Wong, M. W.; Gonzalez, C.; Pople, J. A. *Gaussian 03*, revision D.01; Gaussian, Inc.: Wallingford, CT, 2004.

(17) (a) Cances, E.; Mennucci, B. *J. Math. Chem.* **1998**, *23*, 309. (b) Cances, E.; Mennucci, B.; Tomasi, J. *J. Chem. Phys.* **1997**, *107*, 3032. (c) Mennucci, B.; Cances, E.; Mennucci, B.; Tomasi, J. *J. Phys. Chem. B* **1997**, *101*, 10506.

(18) Oostenbrink, C.; Villa, A.; Mark, A. E.; van Gunsteren, W. F. *J. Comput. Chem.* **2004**, *25*, 1656.

(19) Berendsen, H. J. C.; Postma, J. P. M.; van Gunsteren,W. F.; Hermans, J. Interaction models for water in relation to protein hydration. In *Intermolecular Forces*; Pullman, B., Ed.; Reidel: Dordrecht, 1981; p 331.

(20) (a) Jorgensen, W. L.; Maxwell, D. S.; Tirado-Rives, J. *J. Am. Chem. Soc.* **1996**, *118*, 11225. (b) Kaminski, G. A.; Friesner, R. A.; Tirado-Rives, J.; Jorgensen, W. L. *J. Phys. Chem. B* **2001**, *105*, 6474.

(21) Jorgensen, W. L.; Chandrasekhar, J.; Madura, J. D.; Impey, R. W.; Klein, M. L. *J. Chem. Phys.* **1983**, *79*, 926.

(22) (a) Cornell, W. D.; Cieplak, P.; Bayly, C. I.; Gould, I. R.; Merz, K. M., Jr.; Ferguson, D. M.; Spellmeyer, D. C.; Fox, T.; Caldwell, J. W.; Kollman, P. A. *J. Am. Chem. Soc.* **1995**, *117*, 5179. (b) Wang, J.; Cieplak, P.; Kollman, P. A. *J. Comp. Chem.* **2000**, *21*, 1049. (c) Duan, Y.; Wu, C.; Chowdhury, S.; Lee, M. C.; Xiong, G.; Zhang, W.; Yang, R.; Cieplak, P.; Luo, R.; Lee, T.; Caldwell, J.; Wang, J.; Kollman, P. *J. Comput. Chem.* **2003**, *24*, 1999.

(23) Sorin, E. J.; Pande, V. S. *Biophys. J.* **2005**, *88*, 2472.

(24) Wang, J.; Wolf, R. M.; Caldwell, J. W.; Kollman, P. A.; Case, D. A. *J. Comput. Chem.* **2004**, *25*, 1157.

(25) (a) Lindahl, E.; Hess, B.; van der Spoel, D. *J. Mol. Model.* **2001**, *7*, 306−317. (b) van der Spoel, D.; Lindahl, E.; Hess, B.; Groenhof, G.; Mark, A. E.; Berendsen, H. J. C. *J. Comput. Chem.* **2005**, *26*, 1701.

(26) Case, D. A.; Darden, T. A.; Cheatham, T. E., III; Simmerling, C. L.; Wang, J.; Duke, R. E.; Luo, R.; Merz, K. M.; Pearlman, D. A.; Crowley, M.; Walker, R. C.; Zhang, W.; Wang, B.; Hayik, S.; Roitberg, A.; Seabra, G.; Wong, K. F.; Paesani, F.; Wu, X.; Brozell, S.; Tsui, V.; Gohlke, H.; Yang, L.; Tan, C.; Mongan, J.; Hornak, V.; Cui, G.; Beroza, P.; Mathews, D. H.; Schafmeister, C.; Ross, W. S.; Kollman, P. A. *AMBER 9*, University of California, San Francisco, 2006.

(27) Essman, U.; Perera, L.; Berkowitz, M. L.; Darden, T.; Lee, H.; Pedersen, L. G. *J. Chem. Phys.* **1995**, *103*, 8577.

(28) Tironi, I. G.; Sperb, R.; Smith, P. E.; van Gunsteren, W. F. *J. Chem. Phys.* **1995**, *102*, 5451.

(29) van Gunsteren, W. F.; Berendsen, H. J. C. *Mol. Simul.* **1988**, *1*, 173.

(30) Nose, S. *J. Chem. Phys.* **1984**, *81*, 511.

(31) Hoover, W. *Phys. Rev. A* **1984**, *31*, 1695.

(32) Berendsen, H. J. C.; Postma, J. P. M.; DiNola, A.; Haak, J. R. *J. Chem. Phys.* **1984**, *81*, 3684.

(33) Stewart, J. J. P. *J. Comput. Chem.* **1989**, *10*, 209.

(34) Wang, J.; Wang, W.; Kollman, P. A.; Case, D. A. *J. Mol. Graphics Model.* **2006**, *26*, 247.

(35) Mobley, D. L.; Dumont, E.; Chodera, J. D.; Dill, K. A. *J. Phys. Chem. B* **2007**, *111*, 2242.

(36) (a) Pogliani, L.; Ellenberger, M.; Valat, J. *Org. Magn. Reson.* **1975**, *7*, 61. (b) Anteunis, M. J. O.; Borremans, F. A.; Becu, C.; Sleeckx, J. *Int. J. Pept. Protein Res.* **1979**, *14*, 445.

(37) Altona, C.; Sundaralingam, M. *J. Am. Chem. Soc.* **1972**, *94*, 8205.

(38) Westhof, G.; Sundaralingam, M. *J. Am. Chem. Soc.* **1983**, *105*, 970.

(39) Ramek, M.; Kelterer, A.-M.; Teppen, B. J.; Schafer, L. *J. Mol. Struct.* **1995**, *352/353*, 59.